Revisiting the tsunamigenic volcanic flank collapse of Fogo Island in the Cape Verdes, offshore West Africa

Rachel Barrett[1]*, Elodie Lebas[1], Ricardo Ramalho[2,3,4,5], Ingo Klaucke[6], Steffen Kutterolf[6], Andreas Klügel[7], Katja Lindhorst[1], Felix Gross[1,8] and Sebastian Krastel[1]

[1]Institute of Geosciences, Christian-Albrechts-University, 24118 Kiel, Germany

[2]Instituto Dom Luiz, Faculdade de Ciências da Universidade de Lisboa, 1749-016 Lisbon, Portugal

[3]Departamento de Geologia, Faculdade de Ciências da Universidade de Lisboa, 1749-016 Lisbon, Portugal

[4]School of Earth Sciences, University of Bristol, Bristol BS8 1RL, UK

[5]Lamont-Doherty Earth Observatory of Columbia University, New York, NY 10964, USA

[6]GEOMAR Helmholtz Centre for Ocean Research Kiel, 24148 Kiel, Germany

[7]Department of Geosciences, University of Bremen, 28359 Bremen, Germany

[8]Center for Ocean and Society, Kiel Marine Science, Christian-Albrechts-University, 24118 Kiel, Germany

RB, 0000-0001-6463-4473; EL, 0000-0003-1617-143X; RR, 0000-0002-2338-5535; SKu, 0000-0002-0645-3399; AK, 0000-0002-5136-4774; FG, 0000-0002-0749-829X; SKr, 0000-0002-5899-9748

*Correspondence: rachel.barrett@ifg.uni-kiel.de

Abstract: Volcanic archipelagos are a source of numerous on- and offshore geohazards, including explosive eruptions and potentially tsunamigenic large-scale flank collapses. Fogo Island in the southern Cape Verdes is one of the most active volcanoes in the world, making it both prone to collapse (as evidenced by the *c.* 73 ka Monte Amarelo volcanic flank collapse), and a source of widely distributed tephra and volcanic material. The offshore distribution of the Monte Amarelo debris avalanche deposits and the surrounding volcaniclastic apron were previously mapped using only medium-resolution bathymetric data. Here, using recently acquired, higher-resolution acoustic data, we revisit Fogo's flank collapse and find evidence suggesting that the deposition of hummocky volcanic debris originating from the failed eastern flank most likely triggered the contemporaneous, multi-phase failure of pre-existing seafloor sediments. Additionally, we identify, for the first time, multiple mass-transport deposits in the southern part of the volcaniclastic apron of Fogo and Santiago based on the presence of acoustically chaotic deposits in parametric echo sounder data and volcaniclastic turbiditic sands in recovered cores. These preliminary findings indicate a long and complex history of instability on the southern slopes of Fogo and suggest that Fogo may have experienced multiple flank collapses.

Volcanic archipelagos are home to numerous on- and offshore hazards such as changes in sea-level, storms, volcanic eruptions, slope instabilities, large flank collapses and tsunamis (Casalbore 2018). These events can have devastating consequences for people, nature and infrastructure, both onshore and offshore. A variety of internal and external factors can precondition and trigger flank instabilities. These include: dyke and sill intrusions; volcanic eruptions and tremor; earthquakes; flank over-steepening; the weight of new volcanic material on the island flanks; weakening of the volcanic edifice by weathering and hydrothermal activity and, for smaller landslides, by the effects of wave, wind and storm activity (e.g. Siebert 1984; Begét and Kienle 1992; McGuire 1996, 2003; Murray and Voight 1996; Tibaldi 2001; Cervelli *et al.* 2002; Casalbore *et al.* 2011, 2015; Gross *et al.* 2014; Clare *et al.* 2018). Such factors occur over timescales ranging from seconds to thousands of years and are globally widespread (McGuire 1996; Blahůt *et al.* 2019).

The volume of volcanic flank collapses varies significantly, but can be as large as thousands of cubic kilometres, for example, in the Hawaiian archipelago (Moore *et al.* 1989). Many such events have volumes in the order of tens to hundreds of cubic kilometres, for example at Nisyros Volcano in the Aegean Sea (Tibaldi *et al.* 2008; Livanos *et al.*

From: Georgiopoulou, A., Amy, L. A., Benetti, S., Chaytor, J. D., Clare, M. A., Gamboa, D., Haughton, P. D. W., Moernaut, J. and Mountjoy, J. J. (eds) 2020. *Subaqueous Mass Movements and their Consequences: Advances in Process Understanding, Monitoring and Hazard Assessments*. Geological Society, London, Special Publications, **500**, 13–26.
First published online March 13, 2020, https://doi.org/10.1144/SP500-2019-187

2013), in the Lesser Antilles Arc (Lebas *et al.* 2011; Le Friant *et al.* 2015; Brunet *et al.* 2016), in the Canary Islands (Krastel *et al.* 2001; Masson *et al.* 2002; León *et al.* 2017) and in the Cape Verde Islands (Masson *et al.* 2008). However, even comparatively small-volume volcanic flank collapses, such as the 0.22–0.3 km^3 Anak Krakatau flank collapse in December 2018 (Grilli *et al.* 2019), may result in catastrophic tsunamis. The hazard potential of such flank collapses is widely recognized, but the magnitude, and therefore hazard potential, of the tsunamis that can be triggered by flank collapses is heavily debated (e.g. Moore and Moore 1984; McMurtry *et al.* 2004; Watt *et al.* 2012*a*; Goff *et al.* 2014; Ramalho *et al.* 2015; Paris *et al.* 2018).

Other factors that can contribute to the instability of slopes offshore are the deposition of centimetre- to decimetre-thick discrete layers of volcanic ash across a wide region and the presence of buried turbidites in the volcanic apron. Studies in lacustrine settings (e.g. Wiemer *et al.* 2015; Moernaut *et al.* 2019) and on active offshore margins (e.g. Harders *et al.* 2010; Lafuerza *et al.* 2014; Hornbach *et al.* 2015; Kuhlmann *et al.* 2016; Sammartini *et al.* 2018) have indicated a relationship between tephra layers or turbidites and slide failure planes. Although the exact nature of this relationship is disputed (Wiemer and Kopf 2016), it is thought that tephra could behave as 'weak layers' – layers of inherently lower strength than adjacent layers, which are thereby prone to failure (Locat *et al.* 2014). Using core logging, sedimentological and geotechnical data from the IODP Expedition 340, Lafuerza *et al.* (2014) showed that low hydraulic conductivity of hemipelagic sediments offshore Martinique (Lesser Antilles) could cause low rates of dewatering in turbidites and tephra layers, allowing excess pore fluid pressures to persist at depth. Moreover, Hornbach *et al.* (2015) suggested that even small changes in the stress regime of these layers, such as that resulting from regional strain and grain reorganization during the compaction of sediments, might trigger

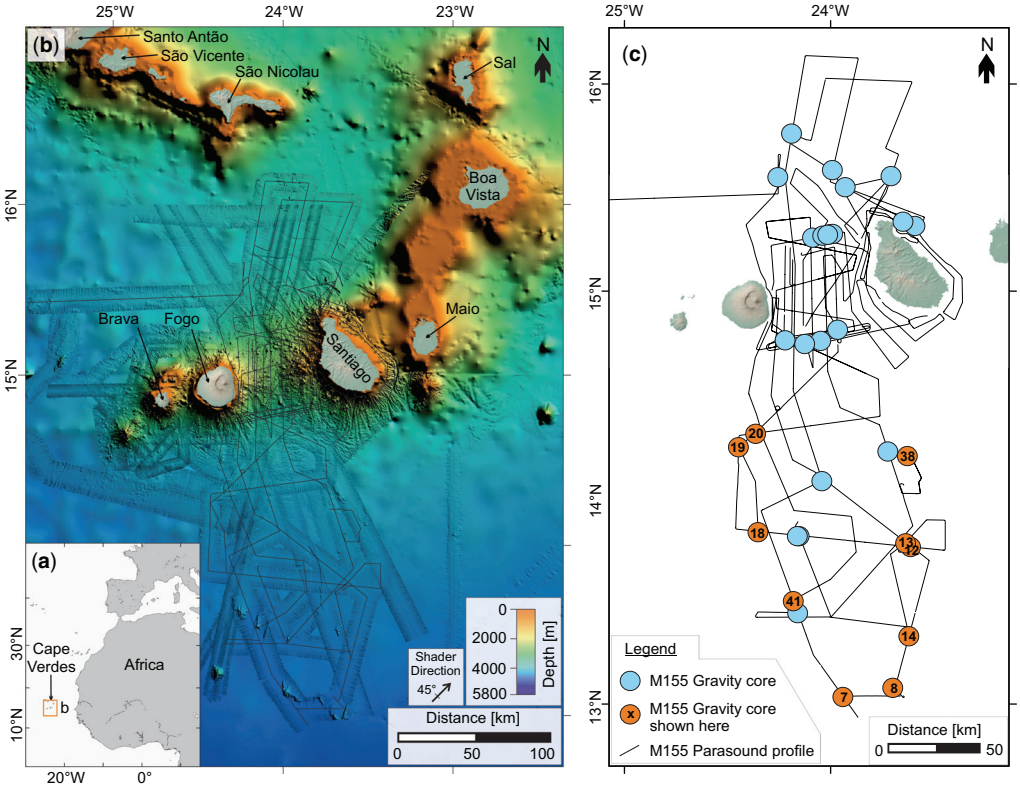

Fig. 1. (**a**) Location of the Cape Verdes offshore West Africa. Box outlines the region presented in (b). (**b**) Multibeam bathymetric data collected during R/V *Meteor* cruises M155 and M80/3 overlain on GEBCO2019 (British Oceanographic Data Centre, http://www.gebco.net) bathymetry of the southern Cape Verdean archipelago. Black lines show the locations of Parasound profiles collected during cruise M155. (**c**) Location of the newly acquired Parasound data and of the gravity cores collected during cruise M155.

motion. Effectively, results from IODP 340 showed that sand layers (i.e. tephra ash and turbidites), as well as boundaries between sand and mud layers, may act as multiple decollement surfaces that promote and enhance the mobility of landslide deposits (Le Friant *et al.* 2015).

Geological setting

The Cape Verdes archipelago, offshore West Africa (Fig. 1), is the surface expression of a mantle hotspot (Crough 1978; Holm *et al.* 2008; Ramalho *et al.* 2010). The Island of Fogo, in the southern part of the archipelago, is one of the most active oceanic intraplate volcanoes in the world, having erupted 28 times in the last 520 years (Ribeiro 1960; Torres *et al.* 1997; González *et al.* 2015). Such volcanically active areas are well known to be associated with seismicity and the southern Cape Verdes are no different, recording frequent volcano-tectonic earthquakes (Grevemeyer *et al.* 2010; Faria and Fonseca 2014; Vales *et al.* 2014). Sediment cores collected in the region provide evidence of at least 43 large, explosive eruptions in the area in the last 150 kyr (Eisele *et al.* 2015), attesting to Fogo's vigorous volcanic activity. Such frequent volcanic activity, along with the accumulation of volcanic deposits on the submarine flanks, means that Fogo's flanks are potentially unstable and prone to collapsing.

A semi-circular depression (Borderia), up to 1 km high and open to the east on central Fogo, was interpreted by Day *et al.* (1999) as the scar of a large flank collapse, referred to as 'Monte Amarelo' (Fig. 2). Other authors, however, interpret the same morphology as two partially overlapping volcanic calderas that were later cut by a flank collapse that affected the eastern portion of the edifice (Brum da Silveira *et al.* 1997; Torres *et al.* 1997; Madeira *et al.* 2008;

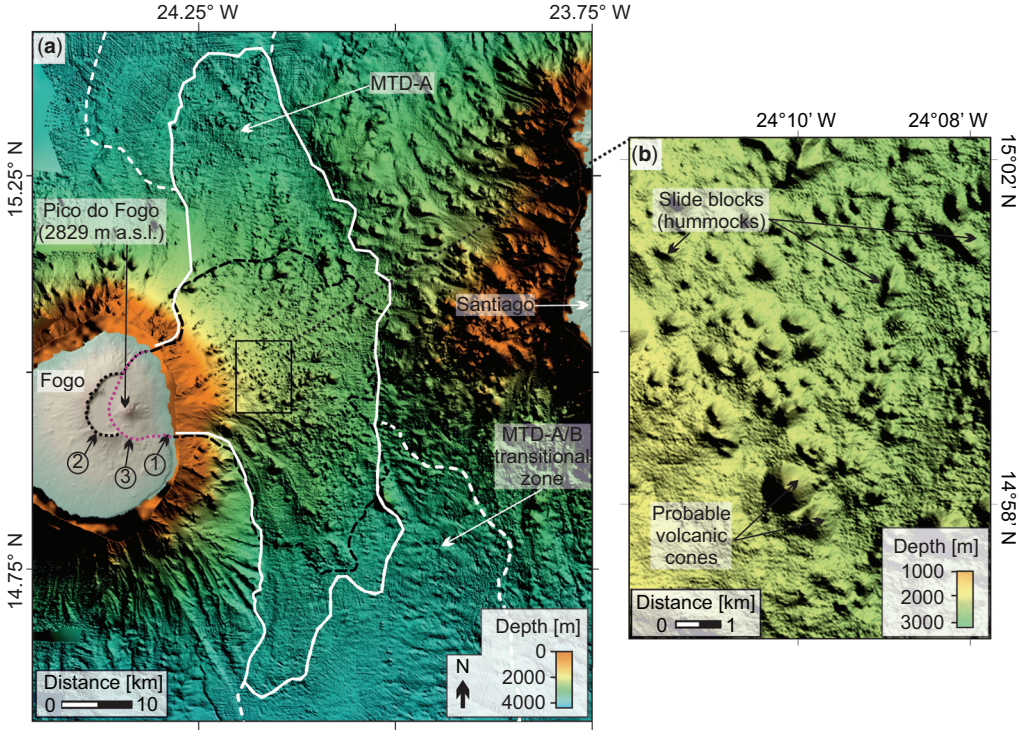

Fig. 2. High-resolution, multibeam bathymetry data highlighting the hummocky nature of the Monte Amarelo debris avalanche deposits (MTD-A) proximal to Fogo. (**a**) Compilation of the M155 and M80/3 multibeam bathymetry data overlain on GEBCO2019 bathymetry and DEM topography of Fogo Island. (1) Espigão escarpment; (2) Bordeira escarpment (dotted black line) is regarded as either the Monte Amarelo headwall scarp (Day *et al.* 1999), or the edge of a caldera (Madeira *et al.* 2008; Martínez-Moreno *et al.* 2018); (3) Monte Amarelo headwall scarp (dotted pink line; Madeira *et al.* 2008; Martínez-Moreno *et al.* 2018); dashed black line: previously estimated extent of the Monte Amarelo debris avalanche deposits (Masson *et al.* 2008); solid white line: revised extent of the Monte Amarelo debris avalanche deposits (MTD-A); dashed white line: transitional zone where the size of the hummocks decreases with distance from the source. (**b**) Enlarged view of the hummocky topography of the Monte Amarelo debris avalanche deposits. Note the angular shape and variable size of the hummocks.

Martínez-Moreno *et al.* 2018). Fogo's Monte Amarelo flank collapse, however, is strongly supported by the presence of a preserved lateral ramp at Espigão (Brum da Silveira *et al.* 1997) and a debris avalanche deposit located between the islands of Fogo and Santiago (Le Bas *et al.* 2007; Masson *et al.* 2008) (Figs 2 & 3). Using a combined magnetotelluric- and multibeam-based approach, Martínez-Moreno *et al.* (2018) estimated a volume of 110 km^3 for the Monte Amarelo debris avalanche deposit. This estimate corresponds well with previous bathymetric-based estimates, which ranged between 80 and 160 km^3 (Le Bas *et al.* 2007; Madeira *et al.* 2008; Masson *et al.* 2008). Tsunami deposits found on the nearby islands of Santiago and Maio indicate that the Monte Amarelo flank collapse was tsunamigenic, with the resulting tsunami achieving a run-up in excess of 270 m above coeval sea-level on Santiago (Ramalho *et al.* 2015; Madeira *et al.* 2019). The exact age of the collapse, however, is the topic of ongoing debate. On the basis of ^{3}He geochronology of lava flows from Fogo, Foeken *et al.* (2009) first estimated the collapse to have occurred between 62 and 123 ka. Paris *et al.* (2011) suggested a narrower window of 86–124 ka, based, respectively, on Ar/Ar ages of lava flows from Fogo thought to be post-collapse, and U–Th dating of corals from tsunami deposits on Santiago. More recently, based on the results of cosmogenic ^{3}He dating of tsunami megaclasts from Santiago Island, Ramalho *et al.* (2015) proposed that the collapse and ensuing tsunami took place between 65 and 84 ka, with a most probable age of 73 $\pm$ 7 ka. This agrees, within uncertainty, with the age recently reported by Maderia *et al.* (2019; 78 $\pm$ 0.9 ka) for a set of tsunami deposits found on the coast of Maio Island. Dating of turbidite material attributed to tsunami-triggered sediment transport along the flanks of Fogo and Brava islands, however, led Eisele *et al.* (2015) to favour an older age of 86–117 ka. Finally, and most recently, Marques *et al.* (2019) suggested a much younger age of 43–59 ka, based on K/Ar dating of Fogo lava flows that they considered to be pre- and post-collapse.

Whether Fogo has collapsed only once or multiple times is also the subject of discussion (Day *et al.* 1999; Ramalho *et al.* 2015; Martínez-Moreno *et al.* 2018; Marques *et al.* 2019). Subsequent eruptions on Fogo have largely been constrained to the central and eastern parts of the island, and a prominent stratovolcano – Pico do Fogo – presently rises to 2829 m above sea-level within the landslide scar (Fig. 2; Torres *et al.* 1997).

Objectives

A detailed analysis of the distribution of the landslide deposits and failure mechanism are critical for constraining the hazard linked to the collapse of a volcanic flank. Moreover, this characterization is crucial for tsunami hazard modelling, given that the mode, volume and run-out of a collapse will have a profound effect on the resulting tsunami waves (Grilli *et al.* 1997; Abadie *et al.* 2012; Watt *et al.* 2012*a*). The offshore distribution of the Monte Amarelo flank-collapse debris (i.e. debris avalanche deposits) and the surrounding volcaniclastic apron were previously mapped using only medium-resolution (100 m grid cell size) multibeam bathymetric data (Masson *et al.* 2008). Consequently, the distribution of the debris avalanche deposits and of any additional slope instabilities in the area are still poorly constrained. As Fogo's volcanic flank collapse likely triggered a mega-tsunami with a recognizable impact on the adjacent islands' coastlines (Paris *et al.* 2011, 2018; Ramalho *et al.* 2015; Madeira *et al.* 2019), a full characterization of this landslide and its related volume is crucial for improving numerical models of tsunami generation, propagation and inundation, and for constraining the hazard potential associated with large, tsunamigenic volcanic flank collapses.

Here, using recently acquired multibeam bathymetric data (50 m grid cell size) in conjunction with parametric sediment echo-sounder data and sediment gravity cores, we revisit the Monte Amarelo volcanic flank collapse and consider general slope stability in the southern distal region of the volcanic apron. We aim to (1) map out the lateral extent and characterize the acoustic nature of the Monte Amarelo debris avalanche deposits; (2) identify possible additional landslides on the slopes south of the islands of Fogo and Santiago; and (3) consider the related preconditioning and triggering processes.

Data and methodology

The data presented in this paper were collected during R/V *Meteor* cruise M155 (May–June 2019; Krastel *et al.* 2019) and are supplemented by multibeam bathymetric data collected during R/V *Meteor* cruise M80/3 (Hansteen *et al.* 2014). The bathymetric data were acquired using hull-mounted Kongsberg EM120 (M80/3), EM122 (M155) and EM710 (M155) multibeam echo-sounders. The EM120/EM122 system has a swath coverage of up to 150° and a nominal sonar frequency of 12 kHz, and is designed to perform seabed mapping to full ocean depth. During cruise M155, the swath width was reduced to 120° in order to increase the quality and resolution of the data. The EM710 system has a swath coverage of up to 140°, and a nominal sonar frequency of 70–100 kHz. As such, the EM710 was used only in water depths less than 700 m close to the islands of Fogo and Santiago. All bathymetric data were filtered for outliers and manually edited. The data

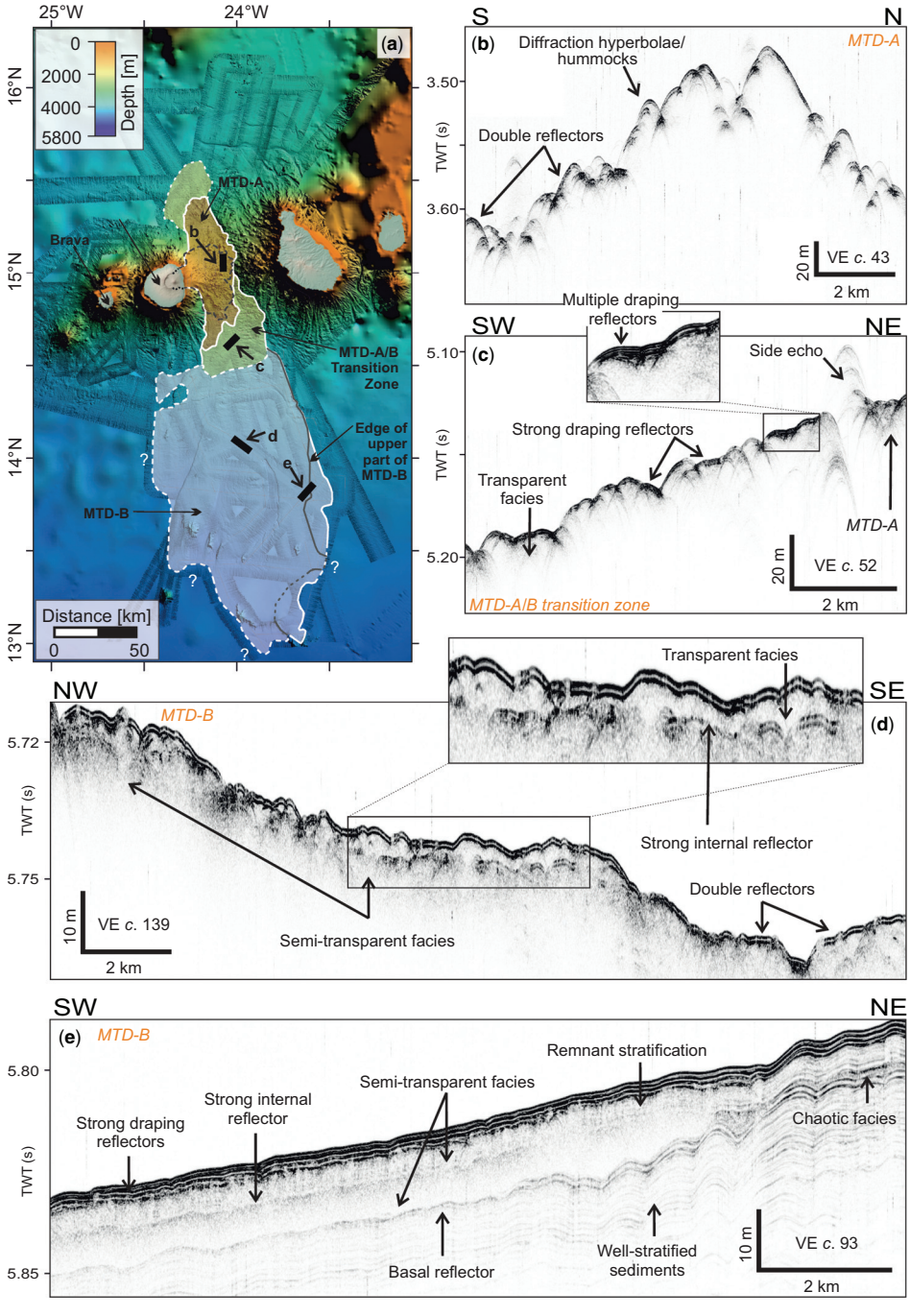

Fig. 3. (**a**) Map showing the distribution of the debris avalanche deposits (MTD-A), the acoustically transparent/ seismically chaotic MTD-B associated with the Monte Amarelo flank collapse, and a transitional zone where the size of the hummocks decreases with distance from the source. The lateral extent of MTD-B may extend further south and west of the surveyed area. Dashed black line: previous mapped extent of the Monte Amarelo deposits (Masson *et al.* 2008); grey line: eastern margin of the upper part of MTD-B; solid black lines: location of the Parasound lines shown in (b)–(e). (**b–e**) Parasound profiles highlighting the acoustic character of (**b**) MTD-A, (**c**) the transitional zone, and (d–e) MTD-B. See the text for discussion on the nature of these deposits. VE, vertical exaggeration.

from all cruises and multibeam systems are combined and gridded at 50 m.

Parametric sediment echo-sounder data were collected using a parametric ATLAS DS-3/P70 system (Parasound). This system has an opening angle of 4° and operates at primary high frequencies of 18.5 and 22.5 kHz, resulting in a parametric low frequency of 4 kHz. The vertical resolution of this system is in the decimetre range. All depth scales on Parasound images presented in this study were calculated using a constant velocity of 1500 m s^{-1}.

Sediment cores were collected during cruise M155 using a gravity corer with tube lengths of 3 to 15 m. These cores were visually described onboard and smear slides were analysed to obtain further microscopic information about the core mineralogy, texture and composition. Dating and further geochemical and sedimentological analysis of these cores is ongoing and will form the basis of future work on the subject.

Results

The Monte Amarelo debris avalanche deposits (MTD-A)

The Monte Amarelo deposits proximal to Fogo (MTD (mass-transport deposit)-A; distribution shown in Fig. 3a) are characterized by overlapping diffraction hyperbolae (Fig. 3b). This hummocky character is typical of debris avalanche deposits from volcanic flank collapses (Siebert 1984). The sedimentary drape covering MTD-A is relatively thin (<1.5 m thick) or not imaged, and is often characterized by two strong, positive reflections. Irregularly shaped blocks that are up to 100 m higher than the surrounding seafloor are present within the landslide debris (Fig. 2). Further away from Fogo, the hummocky topography is less prevalent in the bathymetric data, despite the presence of diffraction hyperbolae in the Parasound data. This highlights a decrease in the size of the hummocks with distance from the island. We note a progressive transition in the acoustic signature of the deposits from a hyperbolic facies with metre-scale acoustic penetration (Fig. 3b), to a mounded facies draped by *c.* 1.5 m of sediment characterized by the aforementioned prominent double reflections (Fig. 3d). In a few places, these double reflections are replaced by a succession of finely stratified layers (inset of Fig. 3c).

Distal deposits related to the Monte Amarelo volcanic flank collapse (MTD-B)

Southwards, with increasing distance from Fogo, the acoustic character of the Monte Amarelo deposits changes from being hyperbolae-dominated to being characterized by an acoustically transparent/semi-transparent facies (Fig. 3d; hereafter referred to as MTD-B; distribution shown in Fig. 3a). In the northern reaches of MTD-B, the upper surface of the deposits is undulating, with metre-scale variations in depth over wavelengths of tens to hundreds of metres (Fig. 3d). The overlying sedimentary drape mantles the surface of the deposits and a strong internal reflector is imaged in places within the deposits (Fig. 3d). This internal reflector clearly contrasts with the overlying transparent facies, separating it from the lower semi-transparent facies. In the northern and western reaches of MTD-B, this internal reflector is either clearly imaged or not present at all, and the base of the lower part of MTD-B is not resolved (Fig. 3d).

In the eastern and southern reaches of MTD-B, the aforementioned internal reflector is continuous over a relatively long distance (Fig. 3e). In these areas, a thicker sedimentary drape (up to *c.* 4 m thick), containing multiple strong reflections alternating with relatively thin, transparent layers, overlies MTD-B. The upper surface of MTD-B is diffuse and undulating in parts. The base of MTD-B is sometimes marked by a prominent reflection that has a similar acoustic signature, although of lower amplitude, as the double reflector that overlies the deposits (e.g. Fig. 3e). A series of well-stratified sediments is imaged below the base of MTD-B (Fig. 3e). At the eastern lateral margin of MTD-B, the internal reflector within the slide deposits is more diffuse (Fig. 3e). The lowermost part of MTD-B remains transparent in nature, but remnant stratifications are imaged in some areas of the uppermost part. The eastern boundary is gradational over 2–3 km, and is marked by a progressive thinning of the transparent facies, and an increase in stratification within the deposits (Fig. 3e).

Constraining the thickness and lateral extent of MTD-B is challenging. In the northern reaches, where the strong internal reflector is imaged, the base of the deposits is not resolved by the acoustic system (Fig. 3c). This means that only the thickness of the upper transparent facies related to MTD-B (up to *c.* 7 m thick, but variable) can be estimated. In its eastern and southern extents, however, the bases of the upper and lower units of MTD-B are imaged, leading to thickness estimates of 4–6 m and 5–15 m for the upper and lower units, respectively (Fig. 3e). The large spacings between the Parasound profiles in the central and southern parts of the working area, south of Fogo and Santiago, mean that we cannot constrain the thickness of the deposits in these areas with certainty. In addition, MTD-B deposits might extend beyond the limits of the surveyed area, especially to the west and south (Fig. 3a).

Additional mass wasting events on the shallow slopes south of Fogo and Santiago

Visual analysis of gravity cores taken in the southern part of the volcaniclastic apron of Fogo and Santiago reveals mud- and nanofossil-rich facies interbedded with multiple sand units that are defined by parallel and cross-laminated, seldom normally graded beds (Fig. 4). These sandy intervals generally range from fine- to coarse-sand deposits, and are typically of centimetre to decimetre scale (Fig. 4b). Microscopic analyses show that these shallow sandy turbidites are predominantly of volcaniclastic (volcanic lithics that are mostly lava fragments, tachylitic to brown glass, crystal fragments), and/or mixed volcaniclastic–bioclastic composition, rather than solely bioclastic.

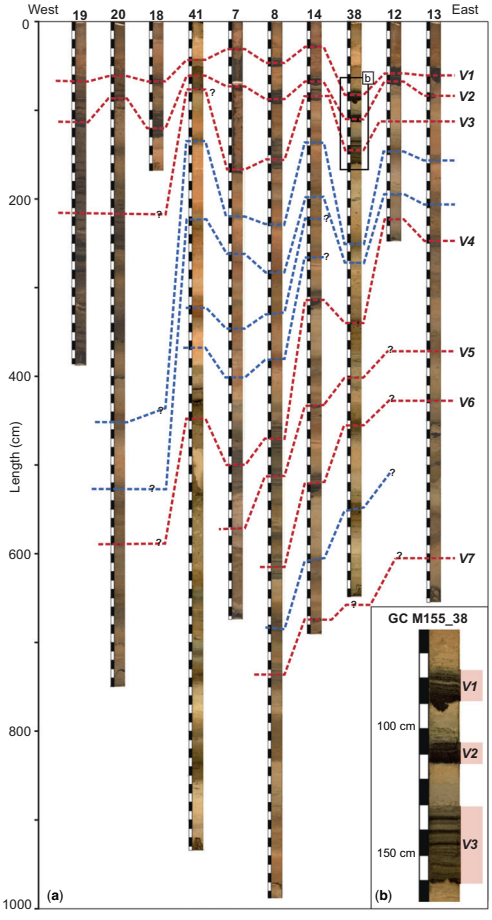

Fig. 4. (**a**) Compilation of sediment gravity cores retrieved south of Fogo and Santiago during M155 showing preliminary stratigraphic correlations based on visual analysis. Dashed red lines: correlations between different volcaniclastic sand layers (V1–V7); dashed blue lines: correlation of background sediment layers (reddish-brown horizons) that helped to correlate the volcaniclastic sand layers. The locations of these cores are shown in Figure 1c. (**b**) Zoom of gravity core M155_38 (62–168 cm) showing the visually identified volcaniclastic layers V1–V3.

Multibeam-bathymetry and sediment echo-sounder data on the shallow slopes south of Fogo and Santiago reveal multiple morphological steps and several MTDs (Fig. 5). These additional MTDs are characterized by acoustically transparent and/or hyperbolic facies and occur both above and below MTD-B. Several of these MTDs are exposed at the surface and have remobilized previously failed sediments, including those of MTD-B (e.g. Figs 5 & 6). However, as for MTD-B, their full lateral extent is generally poorly constrained due to large profile spacings and their possible continuation outside the surveyed area. The morphological steps vary in length, height, strike and orientation (Fig. 5a), but are typically near vertical (Fig. 5c, d). In the following section, we describe the character of, and relation between, several of these features in more detail.

Tectonic escarpments along the western and eastern margins. A series of escarpments is imaged to the west, along the western margin of MTD-B, and stretching between 40 and 110 km south of Fogo (Fig. 5a, b). The most prominent escarpment is orientated roughly north–south and extends across *c.* 55 km. It is *c.* 50 m high and near vertical (Fig. 5c). Monte Amarelo MTD-B deposits are imaged on the eastern side (footwall) of this step. On the western (hanging-wall) side, the sediments are characterized by a semi-transparent facies with a hummocky upper surface (hereafter referred to as MTD-X; Fig. 5c). In places, a pair of strong reflectors is identified within the sedimentary drape that overlies MTD-X. Proximal to the escarpment, the base of MTD-X cannot be resolved. Further west of the scarp, however, stratified sediment is imaged below the base of MTD-X (inset 1 of Fig. 5c). The lateral extent of MTD-X is constrained to both the north and east by the morphological steps (Fig. 5b, c), resulting in a minimum area of 900 km^2 for MTD-X.

Southern Scour Complex. A prominent, elongated scour-shaped feature is evident in the central part of the southern distal region (hereafter referred to as the Southern Scour Complex (SSC), Fig. 6a). This feature is *c.* 60 km long and covers an area of *c.* 340 km^2. The western and eastern sides of the SSC are constrained by up to 40 and 55 m high escarpments, respectively (Fig. 6). In Parasound data crossing the complex, acoustically transparent facies with a strong internal reflector characterizing the Monte Amarelo MTD-B are evident on both the eastern and western sides of the SSC (Fig. 6b & c). In the central part of the SSC (Fig. 6c), acoustically transparent

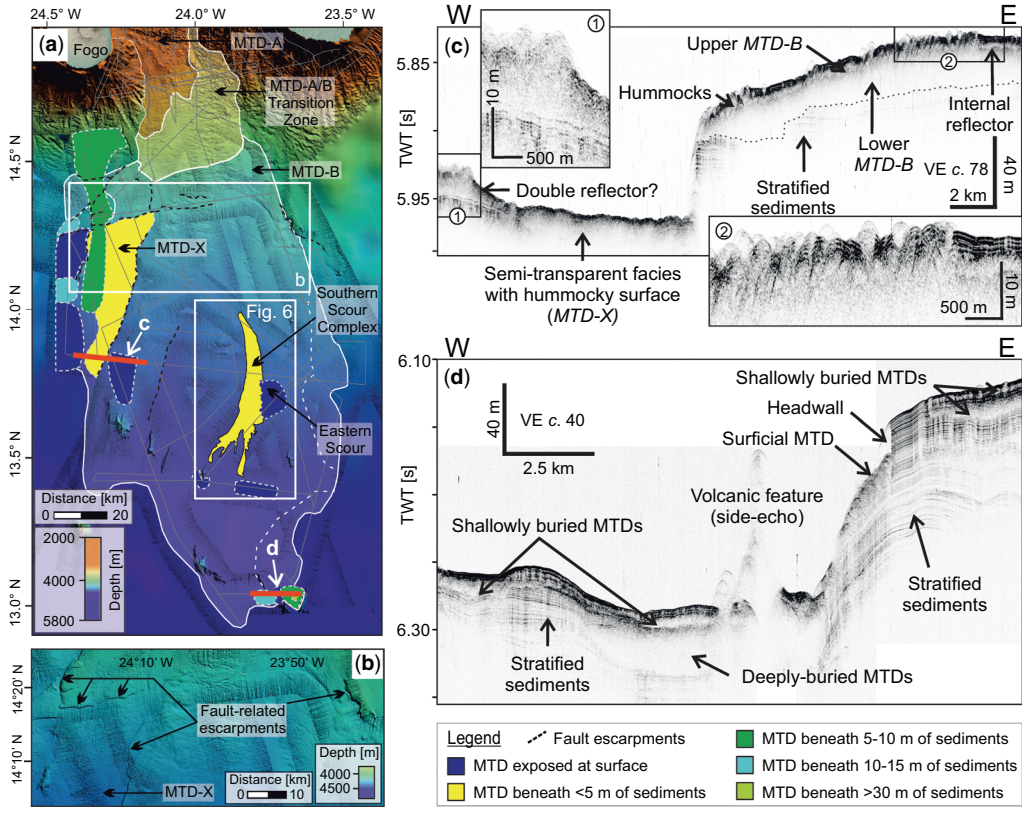

Fig. 5. (**a**) Multibeam data overlain on GEBCO2019 bathymetry highlighting the presence of multiple fault-related escarpments and volcanic features on the shallow slopes south of Fogo. Additional MTDs are also identified in the Parasound data and coloured according to their burial depth (see legend). Solid red lines: location of the Parasound profiles shown in (c) and (d). (**b**) Multibeam data showing the nature of the fault-related escarpments on the slopes south of Fogo and Santiago in more detail. (**c**) Parasound profile crossing one of the most striking escarpments visible on the western side (see (b)), highlights the relation between tectonic processes and landsliding in the area. Monte Amarelo *MTD-B* deposits (eastern side) are remobilized across the escarpment. (**d**) Parasound profile crossing an escarpment in the southern reaches of the working area highlights acoustically transparent MTDs at varying depths.

MTDs with some internal structure are covered by *c.* 3 m of stratified sediment. In the northern part, the material within the SSC is characterized by a semi-transparent facies with a hummocky upper surface, and the deposits are largely exposed at the surface (Fig. 6b). An additional instability is visible on the eastern side of the SSC (hereafter referred to as the Eastern Scour (ES); Fig. 6d). The ES reaches a thickness of up to 35 m thick in its centre and covers an area of *c.* 120 km^2. Parasound data across the ES show that this failure primarily remobilized the Monte Amarelo MTD-B deposits in this region along the same basal glide plane as MTD-B (Fig. 6d). To the south, the SCC is fan-shaped, with fingers of unfailed stratified sediments standing up to *c.* 20 m above failed sediment (Fig. 6d). Semi-transparent deposits characteristic of MTD-B are imaged on the tops of these stratified fingers.

Discussion

The two-fold nature of Fogo's Monte Amarelo flank collapse

Based on the difference in their acoustic character, we distinguish between two main types of deposits related to the Monte Amarelo volcanic flank collapse: hummocky, debris avalanche deposits proximal to Fogo (MTD-A), and finer-grained, acoustically transparent landslide deposits (MTD-B) at greater distances from Fogo that were previously not recognized (Fig. 3). The blocky debris avalanche deposits of MTD-A cover a surface area of 3180 km^2. If we also include the region in which the size of the hummocks decreases with distance from the source (marked by the yellow shaded region in Fig. 3a), this increases the total area of MTD-A to 6820 km^2;

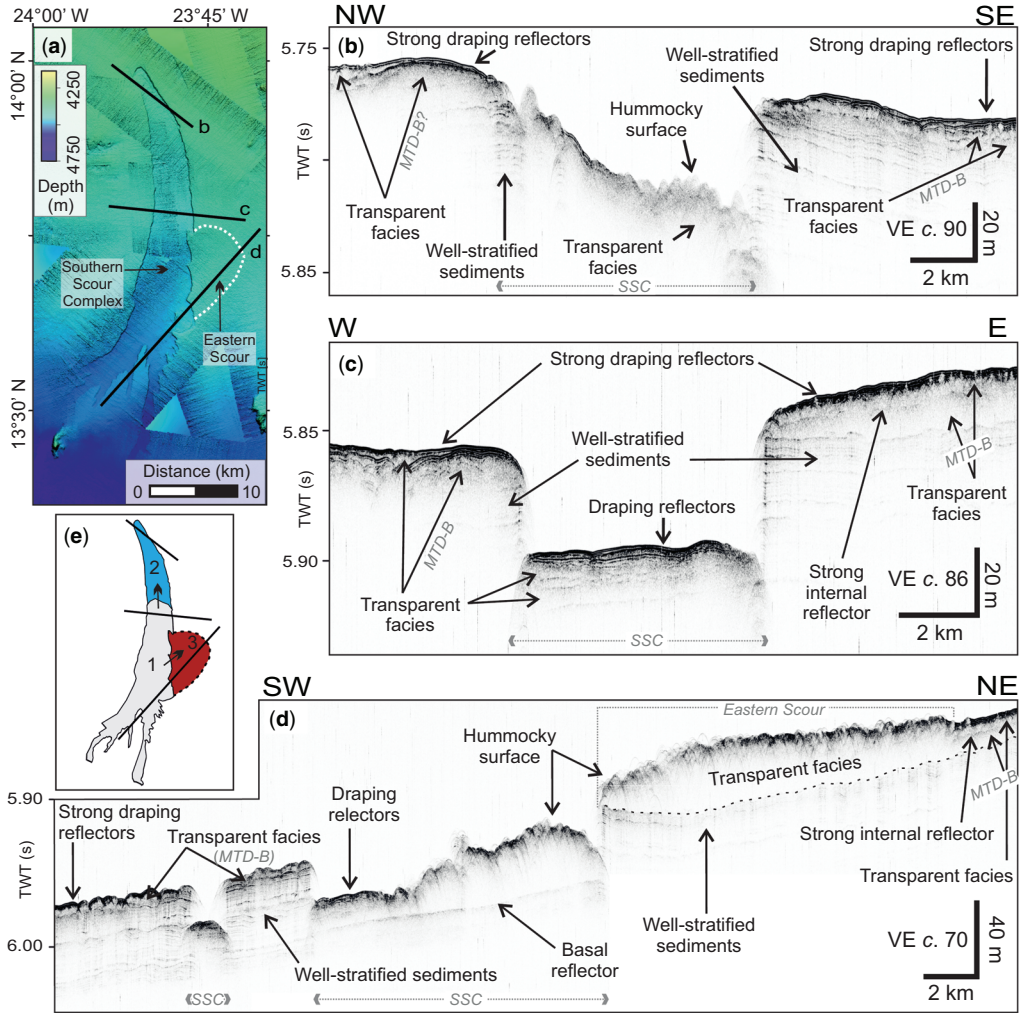

Fig. 6. Southern Scour Complex (SSC). (**a**) Multibeam data highlighting the surface morphology of the SCC and the extension of the Eastern Scour (dashed white line). The location of Figure 6a with respect to the other features discussed in this article is shown in Figure 5. (**b–d**) Parasound profiles crossing the SSC showing a complex relationship between former and more recent landsliding processes, along with the variable acoustic character of the deposits and of the adjacent unfailed material. (**e**) Conceptual model showing the proposed retrogressive development of the SSC towards the north and east. Numbers 1–3 highlight the sequence of events.

more than four times the previous estimate (*c.* 1470 km^2; Masson *et al.* 2008). As the base of the volcanic debris avalanche deposits is not resolved by the Parasound data, we cannot, at this stage, revisit estimates of the volume involved.

Monte Amarelo MTD-B is characterized by an acoustically transparent to semi-transparent facies that is overlain by a series of two to four strong reflectors (Figs 3, 5c & 6b–d). A prominent, internal reflection is clearly observed in places within the deposits; separating MTD-B into two main parts (Fig. 3d, e). The uppermost section is of relatively constant thickness (4–6 m). Contrastingly the thickness of the lower part of MTD-B is highly variable (up to 15 m thick). Interestingly, the upper and lower parts of MTD-B have a similar areal distribution within the volcaniclastic apron; covering a minimum of 18 400 km^2 (upper) and 19 500 km^2 (lower) (Fig. 3a). This implies minimum volumes of 92 km^3 (upper) and 195 km^3 (lower), assuming average thicknesses of 5 m (upper) and 10 m (lower). Their similar distribution implies that the upper and lower parts of MTD-B might share the same source or, at least, be genetically linked. We

therefore infer that the upper and lower part of MTD-B might have been emplaced (almost) contemporaneously. The absolute timing of these two phases, however, remains unclear. Of particular interest is whether these two failures occurred as two phases of the same event, or as two distinct events separated by some time. Further analytical work on the sediment cores will help to reveal more information about the nature of the prominent internal reflection, along with the relative timing of these two depositional episodes.

A similar two-fold nature of volcanic flank-collapse deposits – hummocky debris avalanche deposits accompanied by acoustically transparent to seismically chaotic deposits with a comparatively smooth upper surface – has also been reported for flank collapses at other locations, including in the Lesser Antilles (Watt *et al.* 2012*a*, *b*; Le Friant *et al.* 2015; Brunet *et al.* 2016), at La Réunion (Indian Ocean; Lebas *et al.* 2018) and at Ritter Island (Papua New Guinea; Karstens *et al.* 2019; Watt *et al.* 2019). Drilled cores retrieved during IODP Expedition 340 in the Lesser Antilles indicated that widespread, seismically chaotic deposits (interpreted as equivalent to our MTD-B) primarily consist of hemipelagic mud interbedded with a combination of tephra, volcaniclastic layers, or bioclastic turbiditic deposits, which have undergone varying degrees of deformation (Le Friant *et al.* 2015; Brunet *et al.* 2016). To explain these findings, Le Friant *et al.* (2015) proposed a failure model where the loading of seafloor sediment by volcanic debris avalanche deposits triggered sediment destabilization and progressive downslope-propagating failure along a decollement. In this way, the deformation can propagate great distances away from the flank collapse, affecting seafloor sediments that were otherwise stable (Le Friant *et al.* 2015). The acoustic character of our MTD-B bears a strong resemblance to the seismically chaotic deposits in the Lesser Antilles. We, therefore, interpret MTD-B to be the result of the failure of pre-existing seafloor sediments following the loading of the Monte Amarelo debris avalanche deposits (MTD-A).

A history of mass wasting and remobilization in the southern Cape Verdes

Repeated mass-wasting events at Fogo? Preliminary stratigraphic correlations based on visual similarities of cores in the southern distal part of the working area indicate at least seven volcaniclastic or mixed volcaniclastic–bioclastic sandy turbidite layers above and below the Monte Amarelo flank-collapse deposits (Fig. 4). These turbidite layers are dominated by mafic glass, crystals and lava fragments, which, based on their petrography, suggests that they originated from Fogo volcano. This indicates that smaller mass-wasting events may have occurred at Fogo in addition to the Monte Amarelo volcanic flank collapse, as also recently suggested by Marques *et al.* (2019). Correlation and origin of these volcaniclastic deposits will, however, be verified by future analytical work on the sediment cores.

Regional tectonic and volcanic influences south of Fogo? The multiple fault-related escarpments and MTDs identified in the acoustic data south of Fogo further highlight a long and complex history of instability and slope failure in the region (Fig. 5). Ramalho *et al.* (2010) found that the island of Santiago has uplifted at a rate of *c.* 100 m Ma^{-1} over the past 4 Ma, and attributed this uplift to a combination of magmatic intrusions under or within the island edifice, together with episodic swell-wide uplift that affected the whole archipelago. Although geologically recent uplift has not been reported at Fogo, the neighbouring island of Brava has experienced one of the most dramatic intrusion-related uplift trends of any ocean island in the world, with up to 400 m of uplift in the last 1.8 Ma (Madeira *et al.* 2010). The presence of such widespread uplift across the archipelago – and particularly around the southern Cape Verdes – thus suggests that the series of escarpments and landslides observed on the slopes south of Fogo may be the surface expression of a combination of regional tectonics, associated with the growth of the Cape Verdes hotspot swell, and crustal intrusions in the vicinity of the islands. As several of the exposed faults have landslide deposits on their hanging wall side, we interpret that these MTDs are most likely the results of movement along the faults and, as such, the result of neotectonic activity.

The SSC, which is exposed at the seafloor, postdates the Monte Amarelo flank collapse (Fig. 6). Monte Amarelo MTD-B deposits are imaged on the footwall east of the SSC (Fig. 6b–d), and on the tops of the unfailed, stratified fingers at the southern extent of the SSC (Fig. 6d). This indicates that the SSC formed after the Monte Amarelo flank collapse, remobilizing MTD-B. In the northern and eastern parts of the SSC, acoustically transparent mass-wasting deposits are exposed at the seafloor, highlighting more recent mass wasting and remobilization of MTD-B (Fig. 6b). We interpret the more recent mass-wasting deposits in the northern and eastern parts of the SSC as evidence of retrogressive development of the SSC in these directions (Fig. 6e).

The presence of fault-related escarpments on the slopes south of Fogo, frequent volcanic episodes at Fogo (Ribeiro 1960; Torres *et al.* 1997), and ongoing uplift at the neighbouring islands of Santiago and Brava (Madeira *et al.* 2010; Ramalho *et al.* 2010), together imply the occurrence of frequent

earthquakes in the past. The volcanic activity at Fogo has resulted in the widespread deposition of numerous tephra layers (Eisele *et al.* 2015). Subsequent earthquake shaking may have resulted in liquefaction of overlying layers, which, together with sedimentary overpressure following further sediment deposition, can help to precondition the shallow slopes for failure (Moernaut *et al.* 2019). Even small changes in the stress regime of tephra layers have been found to be able to trigger failure (Hornbach *et al.* 2015). Consequently, it is possible that some of the MTDs observed on the shallowly dipping slopes south of Fogo, and unrelated to escarpments, may result from such a process. Future work, particularly on the sediment cores collected during cruise M155, will help to shed light on the sources and processes responsible for the MTDs mapped on the shallow slopes south of Fogo and Santiago.

Implications and conclusions

In this study, we revisited the Monte Amarelo volcanic flank collapse of Fogo Island and found that the deposition of the debris avalanche material may have triggered subsequent failures of pre-existing seafloor sediments in (at least) two phases. This is similar to what has been observed in the Lesser Antilles (Le Friant *et al.* 2015; Brunet *et al.* 2016), at La Réunion (Lebas *et al.* 2018) and at Ritter Island (Karstens *et al.* 2019; Watt *et al.* 2019). It is not yet clear whether these two phases of seafloor sediment failure were synchronous as a result of a single flank collapse, or if they reflect multiple, distinct events. The question of whether the main flank collapse occurred as a single or as multiple events is of utmost importance for tsunami modelling because the volume and timing of individual failures are the main factors controlling the tsunamigenic potential (Løvholt *et al.* 2015). Water depth and landslide kinematics play a key role in controlling the tsunamigenic potential of a subaqueous landslide (Watts *et al.* 2000; Ward 2001; Watt *et al.* 2012*a*; Harbitz *et al.* 2014). As MTD-B occurred in depths exceeding 3000 m, we consider that its influence on the resulting tsunami magnitude was negligible, and that only the hummocky debris avalanche deposits (MTD-A) contributed to the mega-tsunami that inundated nearby islands.

Multibeam bathymetric, sediment echo-sounder and sediment gravity core data acquired during cruise M155 of R/V *Meteor* provide seafloor evidence that shows, for the first time, the presence of multiple additional mass-wasting events on the shallow slopes south of Fogo. Turbidite sands recovered in the cores have a volcaniclastic or mixed volcaniclastic–bioclastic composition, which suggests that prevailing mass-transport processes in the region may be dominated by volcanic eruptions or volcanic mass-wasting events. However, it is also possible that some of the additional mass-wasting events are unrelated to flank collapse events or submarine failures, and could instead have been generated by sedimentary overpressure and/or by the presence of a mechanically weak layer such as tephra or turbidites. Further analytical work is required to verify the sources of these events on the shallow slopes south of the Cape Verdean archipelago. As these layers are thin, have limited lateral extent and occurred on low-gradient slopes in deep water, we consider their associated tsunamigenic potential to be low.

Acknowledgements We are grateful to the captain, crew and scientific teams of R/V *Meteor* (M155) for their enthusiasm and assistance onboard. We are also thankful for the thoughtful reviews of the editor, Lawrence Amy, as well as Paraskevi Nomikou and two anonymous reviewers, whose comments improved this manuscript.

Funding Data acquisition during R/V *Meteor*'s cruise M155 was funded by the DFG and BMBF. R. Barrett is funded by the European Union's Horizon 2020 research and innovation programme under the Marie Skłodowska-Curie grant agreement No. 721403 (SLATE – 'Submarine LAndslides and Their impact on European continental margins'). R. Ramalho acknowledges his IF/01641/2015 contract funded by Fundação para a Ciência e Tecnologia (FCT), as well as the following projects funded by FCT: IF/01641/2015, LISBOA-01-0145-FEDER-028588 and PTDC/CTA-GEO/28588/2017 UNTIeD, PTDC/GEO-GEO/1123/2014 FIRE, and UID/GEO/50019/2019 – Instituto Dom Luiz.

Author contributions **RB**: conceptualization (lead), formal analysis (lead), investigation (supporting), methodology (lead), validation (lead), visualization (lead), writing – original draft (lead), writing – review & editing (lead); **EL**: conceptualization (supporting), formal analysis (supporting), investigation (supporting), methodology (supporting), project administration (supporting), supervision (supporting), validation (supporting), visualization (supporting), writing – review & editing (supporting); **RR**: conceptualization (supporting), formal analysis (supporting), funding acquisition (supporting), investigation (supporting), project administration (supporting), writing – review & editing (supporting); **IK**: conceptualization (supporting), formal analysis (supporting), investigation (supporting), project administration (supporting), writing – review & editing (supporting); **SKu**: conceptualization (supporting), data curation (equal), formal analysis (supporting), funding acquisition (supporting), investigation (supporting), project administration (supporting), writing – review & editing (supporting); **AK**: conceptualization (supporting), formal analysis (supporting), funding acquisition (supporting), investigation (supporting), project administration (supporting), writing – review & editing (supporting); **KL**: conceptualization (supporting), formal analysis

(supporting), investigation (supporting), writing – review & editing (supporting); **FG**: conceptualization (supporting), formal analysis (supporting), methodology (supporting), supervision (supporting), writing – review & editing (supporting); **SKr**: conceptualization (supporting), data curation (lead), formal analysis (supporting), funding acquisition (lead), investigation (lead), project administration (lead), supervision (lead), validation (supporting), writing – review & editing (supporting).

References

Abadie, S.M., Harris, J.C., Grilli, S.T. and Fabre, R. 2012. Numerical modeling of tsunami waves generated by the flank collapse of the Cumbre Vieja Volcano (La Palma, Canary Islands): tsunami source and near field effects. *Journal of Geophysical Research: Oceans*, **117**, 1–26, https://doi.org/10.1029/2011JC007646

Begét, J.E. and Kienle, J. 1992. Cyclic formation of debris avalanches at Mount St Augustine volcano. *Nature*, **356**, 701–704, https://doi.org/10.1038/35670la0

Blahůt, J., Balek, J., Klimeš, J., Rowberry, M., Kusák, M. and Kalina, J. 2019. A comprehensive global database of giant landslides on volcanic islands. *Landslides*, **16**, 2045–2052, https://doi.org/10.1007/s10346-019-01275-8

Brum da Silveira, A., Madeira, J., Serralheiro, A., Torres, P.C., da Silva, L.C. and Mendes, M.H. 1997. O controlo estrutural da erupção de Abril de 1995 na Ilha do Fogo, Cabo Verde. *In*: *A Erupção Vulcânica de 1995 na Ilha do Fogo, Cabo Verde*. Publ. IICT, Lisbon, 51–61.

Brunet, M., Le Friant, A. *et al*. and IODP Expedition 340 Science Party. 2016. Composition, geometry, and emplacement dynamics of a large volcanic island landslide offshore Martinique: from volcano flank- collapse to seafloor sediment failure? *Geochememistry, Geophysics, Geosystems*, **17**, 699–724, https://doi.org/10.1002/2015GC006034

Casalbore, D. 2018. Volcanic islands and seamounts. *In*: Micallef, A., Krastel, S. and Savini, A. (eds) *Submarine Geomorphology*. Springer Geology. Springer, Cham, 333–347, https://doi.org/10.1007/978-3-319-57852-1_17

Casalbore, D., Romagnoli, C., Bosman, A. and Chiocci, F.L. 2011. Potential tsunamigenic landslides at Stromboli Volcano (Italy): insight from marine DEM analysis. *Geomorphology*, **126**, 42–50, https://doi.org/10.1016/j.geomorph.2010.10.026

Casalbore, D., Romagnoli, C. *et al*. 2015. Volcanic, tectonic and mass-wasting processes offshore Terceira Island (Azores) revealed by high-resolution seafloor mapping. *Bulletin of Volcanology*, **77**, 1–19, https://doi.org/10.1007/s00445-015-0905-3

Cervelli, P., Segall, P., Johnson, K., Lisowski, M. and Miklius, A. 2002. Sudden aseismic fault slip on the south flank of Kilauea volcano. *Nature*, **415**, 1014–1018, https://doi.org/10.1038/4151014a

Clare, M.A., Le Bas, T. *et al*. 2018. Complex and cascading triggering of submarine landslides and turbidity currents at volcanic islands revealed from integration of high-resolution onshore and offshore surveys. *Frontiers in Earth Science*, **6**, https://doi.org/10.3389/feart.2018.00223

Crough, S.T. 1978. Thermal origin of mid-plate hot-spot swells. *Geophysical Journal of the Royal Astronomical Society*, **55**, 451–469, https://doi.org/10.1111/j.1365-246X.1978.tb04282

Day, S.J., Heleno da Silva, S.I.N. and Fonseca, J.F.B.D. 1999. A past giant lateral collapse and present-day flank instability of Fogo, Cape Verde Islands. *Journal of Volcanology and Geothermal Research*, **94**, 191–218, https://doi.org/10.1016/S0377-0273(99)00103-1

Eisele, S., Reißig, S., Freundt, A., Kutterolf, S., Nürnberg, D., Wang, K.L. and Kwasnitschka, T. 2015. Pleistocene to Holocene offshore tephrostratigraphy of highly explosive eruptions from the southwestern Cape Verde Archipelago. *Marine Geology*, **369**, 233–250, https://doi.org/10.1016/j.margeo.2015.09.006

Faria, B. and Fonseca, J.F.B.D. 2014. Investigating volcanic hazard in Cape Verde Islands through geophysical monitoring: network description and first results. *Natural Hazards Earth System Sciences*, **14**, 485–499, https://doi.org/10.5194/nhess-14-485-2014

Foeken, J.P.T., Day, S. and Stuart, F.M. 2009. Cosmogenic ^{3}He exposure dating of the Quaternary basalts from Fogo, Cape Verdes: implications for rift zone and magmatic reorganization. *Quaternary Geochronology*, **4**, 37–49, https://doi.org/10.1016/j.quageo.2008.07.002

Goff, J., Terry, J.P., Chagué-Goff, C. and Goto, K. 2014. What is a mega-tsunami? *Marine Geology*, **358**, 12–17, https://doi.org/10.1016/j.margeo.2014.03.013

González, P.J., Bagnardi, M., Hooper, A.J., Larsen, Y., Marinkovic, P., Samsonov, S.V. and Wright, T.J. 2015. The 2014–2015 eruption of Fogo volcano: geodetic modeling of Sentinel-1 TOPS interferometry. *Geophysical Research Letters*, **42**, 9239–9246, https://doi.org/10.1002/2015GL066003

Grevemeyer, I., Helffrich, G., Faria, B., Booth-Rea, G., Schnabel, M. and Weinrebe, W. 2010. Seismic activity at Cadamosto seamount near Fogo Island, Cape Verdes: formation of a new ocean island? *Geophysical Journal International*, **180**, 552–558, https://doi.org/10.1111/j.1365-246X.2009.04440.x

Grilli, S.T., Svendsen, I.A. and Subramanya, R. 1997. Breaking criterion and characteristics for solitary waves on slopes. *Journal of Waterway, Port, Coastal, and Ocean Engineering*, **123**, 102–112, https://doi.org/10.1061/(ASCE)0733-950X(1997)123:3(102)

Grilli, S.T., Tappin, D.R. *et al*. 2019. Modelling of the tsunami from the December 22, 2018 lateral collapse of Anak Krakatau volcano in the Sunda Straits, Indonesia. *Science Reports*, **9**, 11946, https://doi.org/10.1038/s41598-019-48327-6

Gross, F., Krastel, S. *et al*. 2014. Evidence for submarine landslides offshore Mt. Etna, Italy. *In*: Krastel, S. *et al*. (eds) *Submarine Mass Movements and Their Consequences*. Advances in Natural and Technological Hazards Research, **37**. Springer, Cham, 307–316, https://doi.org/10.1007/978-3-319-00972-8_27

Hansteen, T.H., Kwasnitschka, T. and Klügel, A. 2014. *Cape Verde Seamounts – Cruise No. M80/3 – December 29 2009 – February 1 2010 – Dakar (Senegal) – Las Palmas de Gran Canaria (Spain)*. METEOR-Berichte, **M80/3**, DFG-Senatskommission für Ozeanographie, Bremen, https://doi.org/10.2312/cr_m80_3

Harbitz, C.B., Løvholt, F. and Bungum, H. 2014. Submarine landslide tsunamis: how extreme and how likely?. *Natural Hazards*, **72**, 1341–1374, https://doi.org/10.1007/s11069-013-0681-3

Harders, R., Kutterolf, S., Hensen, C., Moerz, T. and Brueckmann, W. 2010. Tephra layers: a controlling factor on submarine translational sliding?. *Geochemistry, Geophysics, Geosystems*, **11**, 1–18, https://doi.org/10.1029/2009GC002844

Holm, P.M., Grandvuinet, T., Friis, J., Wilson, J.R., Barker, A.K. and Plesner, S. 2008. An ^{40}Ar-^{39}Ar study of the Cape Verde hot spot: temporal evolution in a semistationary plate environment. *Journal of Geophysical Research*, **113**, 1–22, https://doi.org/10.1029/2007JB005339

Hornbach, M.J., Manga, M. *et al*. 2015. Permeability and pressure measurements in Lesser Antilles submarine slides: evidence for pressure-driven slow-slip failure. *Journal of Geophysical Research: Solid Earth*, **120**, 7986–8011, https://doi.org/10.1002/2015JB012061

Krastel, S., Schmincke, H.-U., Jacobs, C.L., Rihm, R., Le Bas, T.P. and Alibes, B. 2001. Submarine landslides around the Canary Islands. *Journal of Geophysical Research*, **106**, 3977–3998, https://doi.org/10.1029/2000JB900413

Krastel, S., Andrade, M. *et al*. 2019. *The tsunamigenic gravitational flank-collapse of Fogo volcano, Cape Verde Islands, Seismic pre-site survey for an IODP site on the Cape Verde Plateau, Cruise No. M155, 26.05.19–30.06.19, Pointe-à-Pitre (Guadeloupe) – Mindelo (Cape Verde)*. METEOR-Berichte, Gutachterpanel Forschungsschiffe, Bonn, **M155**, 1–44, https://doi.org/10.2312/cr_m155

Karstens, J., Berndt, C. *et al*. 2019. From gradual spreading to catastrophic collapse: Reconstruction of the 1888 Ritter Island volcanic sector collapse from high-resolution 3D seismic data. *Earth and Planetary Science Letters*, **517**, 1–13, https://doi.org/10.1016/j.epsl.2019.04.009

Kuhlmann, J., Huhn, K. and Ikari, M.J. 2016. Do embedded volcanoclastic layers serve as potential glide planes? An integrated analysis from the Gela Basin offshore southern Sicily. *In*: Lamarche, G. *et al*. (eds) *Submarine Mass Movements and Their Consequences*. Advances in Natural and Technological Hazards Research, **41**. Springer, Cham, 273–280, https://doi.org/10.1007/978-3-319-20979-1_27

Lafuerza, S., Le Friant, A. and the Expedition 340 Scientific Party 2014. Geomechanical characterizations of submarine volcano flank sediments, Martinique, Lesser Antilles Arc. *In*: Krastel, S. *et al*. (eds) *Submarine Mass Movements and Their Consequences*. Advances in Natural and Technological Hazards Research, **37**. Springer, Cham, https://doi.org/10.1007/978-3-319-00972-8_7

Lebas, E., Le Friant, A. *et al*. 2011. Multiple widespread landslides during the long-term evolution of a volcanic island: insights from high-resolution seismic data. Montserrat, Lesser Antilles. *Geochemistry, Geophysics, Geosystems*, **12**, https://doi.org/10.1029/2010GC003451

Lebas, E., Le Friant, A., Deplus, C. and de Voogd, B. 2018. Understanding the evolution of an oceanic intraplate volcano from seismic reflection data: a new model for La Réunion, Indian Ocean. *Journal of Geophysical Research*, **123**, 1035–1059, https://doi.org/10.1002/2017JB014959

Le Bas, T.P., Masson, D.G., Holtom, R.T. and Grevemeyer, I. 2007. Slope failures of the flanks of the southern Cape Verde Islands. *In*: Lykousis, V., Sakellariou, D. and Locat, J. (eds) *Submarine Mass Movements and Their Consequences*. Advances in Natural and Technological Hazards Research, **27**. Springer, Dordrecht, 337–345, https://doi.org/10.1007/978-1-4020-6512-5_35

Le Friant, A., Ishizuka, O., Boudon, G. *et al*. 2015. Submarine record of volcanic island construction and collapse in the Lesser Antilles arc: first scientific drilling of submarine volcanic island landslides by IODP Expedition 340. *Geochemistry, Geophysics, Geosystems*, **16**, 420–442, https://doi.org/10.1002/2014GC005652

León, R., Somoza, L. *et al*. 2017. Multi-event oceanic island landslides: new onshore-offshore insights from El Hierro Island, Canary Archipelago. *Marine Geology*, **393**, 156–175, https://doi.org/10.1016/j.margeo.2016.07.001

Livanos, I., Nomikou, P., Papanikolaou, D. and Rousakis, G. 2013. The volcanic debris avalanche on the SE submarine slope of Nisyros volcano, Greece: geophysical exploration and implications for subaerial eruption history. *Geo-Marine Letters*, **33**, 419, https://doi.org/10.1007/s00367-013-0338-y

Locat, J., Leroueil, S., Locat, A. and Lee, H.J. 2014. Weak layers: their definition and classification from a geotechnical perspective. *In*: Krastel, S. *et al*. (eds) *Submarine Mass Movements and Their Consequences*. Advances in Natural and Technological Hazards Research, **37**. Springer, Cham, 3–12, https://doi.org/10.1007/978-3-319-00972-8_1

Løvholt, F., Pedersen, G., Harbitz, C.B., Glimsdal, S. and Kim, J. 2015. On the characteristics of landslide tsunamis. *Philosophical Transactions of the Royal Society A*, **373**, https://doi.org/10.1098/rsta.2014.0376

Madeira, J., Brum da Silveira, A., Mata, J., Mourão, C. and Martins, S. 2008. The role of mass movements on the geomorphologic evolution of island volcanoes: examples from Fogo and Brava in the Cape Verde archipelago. *Comunicações Geológicas*, **95**, 93–106.

Madeira, J., Mata, J., Mourão, C., Brum dal Silveira, A., Martins, S., Ramalho, R. and Hoffman, D.L. 2010. Volcano-stratigraphic and structural evolution of Brava Island (Cape Verde) based on ^{40}Ar/^{39}Ar, U–Th and field constraints. *Journal of Volcanology and Geothermal Research*, **196**, 219–235, https://doi.org/10.1016/j.jvolgeores.2010.07.010

Madeira, J., Ramalho, R.S., Hoffmann, D.L., Mata, J. and Moreira, M. 2019. A geological record of multiple Pleistocene tsunami inundations in an oceanic island: the case of Maio, Cape Verde. *Sedimentology*, https://doi.org/10.1111/sed.12612

Marques, F.O., Hildenbrand, A., Victória, S.S., Cunha, C. and Dias, P. 2019. Caldera or flank collapse in the Fogo volcano? What age? Consequences for risk assessment in volcanic islands. *Journal of Volcanology and Geothermal Research*, **388**, 106686. https://doi.org/10.1016/j.jvolgeores.2019.106686

Martínez-Moreno, F.J., Monteiro Santos, F.A. *et al*. 2018. Investigating collapse structures in oceanic islands using magnetotelluric surveys: the case of Fogo Island in Cape Verde. *Journal of Volcanology and*

Geothermal Research, **357**, 152–162, https://doi.org/10.1016/j.jvolgeores.2018.04.028

Masson, D.G., Watts, A.B., Gee, M.J.R., Urgeles, R., Mitchell, N.C., Le Bas, T.P. and Canals, M. 2002. Slope failures on the flanks of the western Canary Islands. *Earth-Science Reviews*, **57**, 1–35, https://doi.org/10.1016/S0012-8252(01)00069-1

Masson, D.G., Le Bas, T.P., Grevemeyer, I. and Weinrebe, W. 2008. Flank collapse and large-scale landsliding in the Cape Verde Islands, off West Africa. *Geochemistry, Geophysics, Geosystems*, **9**, 16, https://doi.org/10.1029/2008GC001983

McGuire, W.J. 1996. Volcano instability: a review of contemporary themes. *Geological Society, London, Special Publications*, **110**, 1–23, https://doi.org/10.1144/GSL.SP.1996.110.01.01

McGuire, W.J. 2003. Volcano instability and lateral collapse. *Revista*, **1**, 33–45.

McMurtry, G.M., Fryer, G.J. *et al*. 2004. Megatsunami deposits on Kohala volcano, Hawaii, from flank collapse of Mauna Loa. *Geology*, **32**, 741–744, https://doi.org/10.1130/G20642.1

Moernaut, J., Van Daele, M. *et al*. 2019. The subaqueous landslide cycle in south-central Chilean lakes: the role of tephra, slope gradient and repeated seismic shaking. *Sedimentary Geology*, **381**, 84–105, https://doi.org/10.1016/j.sedgeo.2019.01.002

Moore, J.G. and Moore, G.W. 1984. Deposit from a giant wave on the island of Lanai, Hawaii. *Science*, **226**, 1312–1315, https://doi.org/10.1126/science.226.4680.1312

Moore, J.G., Clague, D.A., Holcomb, R.T., Lipman, P.W., Normark, W.R. and Torresan, M.E. 1989. Prodigious submarine landslides on the Hawaiian Ridge. *Journal of Volcanology and Geothermal Research*, **94**, 17465–17485, https://doi.org/10.1029/JB094iB12p17465

Murray, J.B. and Voight, B. 1996. Slope stability and eruption prediction on the eastern flank of Mount Etna. *Geological Society, London, Special Publications*, **110**, 111–114, https://doi.org/10.1144/GSL.SP.1996.110.01.08

Paris, R., Geichetti, T., Chevalier, J., Guillou, H. and Frank, N. 2011. Tsunami deposits in Santiago Island (Cape Verde archipelago) as possible evidence of a massive flank failure of Fogos volcano. *Sedimentary Geology*, **239**, 129–145, https://doi.org/10.1016/j.sedgeo.2011.06.006

Paris, R., Ramalho, R.S. *et al*. 2018. Mega-tsunami conglomerates and flank collapses of ocean island volcanoes. *Marine Geology*, **395**, 168–187, https://doi.org/10.1016/j.margeo.2017.10.004

Ramalho, R., Helffrich, G., Cosca, M., Vance, D., Hoffmann, D. and Schmidt, D.N. 2010. Episodic swell growth inferred from variable uplift of the Cape Verde hotspot islands. *Nature Geoscience*, **3**, 774–777, https://doi.org/10.1038/NGEO982

Ramalho, R.S., Winckler, G. *et al*. 2015. Hazard potential of volcanic flank collapses raised by new megatsunami evidence. *Scientific Advances*, **1**, e1500456, https://doi.org/10.1126/sciadv.1500456

Ribeiro, O. 1960. *A ilha do Fogo e as suas erupiones*. 2nd edn. Memorias, serie geografica I. Publ. Junta de Investigacoes do Ultramar, Ministerio do Ultramar, Lisbon.

Sammartini, M., Camerlenghi, A. *et al*. 2018. Open-slope, translational submarine landslide in a tectonically active volcanic continental margin (Licosa submarine landslide, southern Tyrrhenian Sea). *Geological Society, London, Special Publications*, **477**, 133–150, https://doi.org/10.1144/SP477.34

Siebert, L. 1984. Large volcanic debris avalanches: characteristics of source areas, deposits, and associated eruptions. *Journal of Volcanology and Geothermal Research*, **22**, 163–197, https://doi.org/10.1016/0377-0273(84)90002-7

Tibaldi, A. 2001. Multiple sector collapses at Stromboli volcano, Italy: how they work. *Bulletin of Volcanology*, **63**, 112–125, https://doi.org/10.1016/S1464-1909(99)00022-2

Tibaldi, A., Pasquarè, F.A., Papanikolaou, D. and Nomikou, P. 2008. Discovery of a huge sector collapse at the Nisyros volcano, Greece, by on-land and offshore geological-structural data. *Journal of Volcanology and Geothermal Research*, **177**, 485, https://doi.org/10.1016/j.jvolgeores.2008.06.014

Torres, P., Madeira, J., Silva, L., Brum da Silveira, A., Serralheiro, A. and Mota Gomes, A. 1997. *Carta geológica das erupções históricas da Ilha do Fogo: revisão e actualização: A erupcao vulcanica de 1995 na Ilha do Fogo, Cabo Verde*. Publ IICT, Lisbon, 119–132.

Vales, D., Dias, N.A. *et al*. 2014. Intraplate seismicity across the Cape Verde swell: a contribution from a temporary seismic network. *Tectonophysics*, **636**, 325–337, https://doi.org/10.1016/j.tecto.2014.09.014

Ward, S.N. 2001. Landslide tsunami. *Journal of Geophysical Research*, **106**, 11201–11215, https://doi.org/10.1029/2000JB900450

Watt, S.F.L., Talling, P.J. *et al*. 2012*a*. Combinations of volcanic-flank and seafloor-sediment failure offshore Montserrat, and their implications for tsunami generation. *Earth and Planetary Science Letters*, **319**, 228–240, https://doi.org/10.1016/j.epsl.2011.11.032

Watt, S.F.L., Talling, P.J. *et al*. 2012*b*. Widespread and progressive seafloor-sediment failure following volcanic debris avalanche emplacement: landslide dynamics and timing offshore Montserrat, Lesser Antilles. *Marine Geology*, **323–325**, 69–94, https://doi.org/10.1016/j.margeo.2012.08.002

Watt, S.F.L., Karstens, J. *et al*. 2019. From catastrophic collapse to multi-phase deposition: flow transformation, seafloor interaction and triggered eruption following a volcanic-island landslide. *Earth and Planetary Science Letters*, **517**, 135–147, https://doi.org/10.1016/j.epsl.2019.04.024

Watts, P., Imamura, F. and Grilli, S.T. 2000. Comparing model simulations of three benchmark tsunami generation cases. *Science of Tsunami Hazards*, **18**, 107–124.

Wiemer, G. and Kopf, A. 2016. On the role of volcanic ash deposits as preferential submarine slope failure planes. *Landslides*, **14**, https://doi.org/10.1007/s10346-016-0706-6

Wiemer, G., Moernaut, J. *et al*. 2015. The role of sediment composition and behaviour under dynamic loading conditions on slope failure initiation: a study of a subaqueous landslide in earthquake-prone South-Central Chile. *International Journal of Earth Sciences*, **104**, 1439–1457, https://doi.org/10.1007/s00531-015-1144-8